Catalysis Today 119 (2007), p. 187-193

The effect of the Rh–Al, Pt–Al and Pt–Rh–Al surface alloys on NO conversion to N_2 on alumina supported Rh, Pt and Pt–Rh catalysts

A. Pietraszek[a], P. Da Costa[b], R. Marques[b], P. Kornelak[a], T.W. Hansen[c], J. Camra[d] and M. Najbar[a,*]

[a]Department of Chemistry, Jagiellonian University, 30-060 Kraków, Ingardena 3, Poland
[b]Laboratoire de Réactivité de Surface, Université P. et M. Curie, 4 Place Jussieu, 75 252 Paris Cedex 05, France
[c]Fritz Haber Institut der Max Planck Gesellschaft, Faradayweg 4-6, D-14195 Berlin, Germany
[d]Regional Laboratory of Physicochemical Analyses and Structural Research, 30-060 Kraków, Ingardena 3, Poland

[*] e-mail: mnajbar@chemia.uj.edu.pl

Abstract

NO conversion to N_2 in the presence of methane and oxygen over 0.03 at.% Rh/Al_2O_3, 0.51 at.% Pt/Al_2O_3 and 0.34 at.% Pt–0.03 at.% Rh/Al_2O_3 catalysts was investigated.
δ-Alumina and precious metal–aluminum alloy phases were revealed by XRD and HRTEM in the catalysts.
The results of the catalytic activity investigations, with temperature-programmed as well as steady-state methods, showed that NO decomposition occurs at a reasonable rate on the alloy surfaces at temperatures up to 623 K whereas some CH_4 $deNO_x$ takes place on δ-alumina above this temperature. A mechanism for the NO decomposition is proposed herein. It is based on NO adsorption on the precious metal atoms followed by the transfer of electrons from alloy to antibonding π orbitals of $NO_{(ads.)}$ molecules. The CH_4 $deNO_x$ was shown to occur according to an earlier proposed mechanism, via methane oxidation by $NO_{2(ads.)}$ to oxygenates and then NO reduction by oxygenates to N_2.

Keywords: Rh–Al, Pt–Al and Pt–Rh–Al alloys; NO decomposition; CH_4 $deNO_x$

1. Introduction

The removal of NO_x (NO and NO_2) from oxygen-containing off-gases of stationary and mobile sources of emission is a fundamental problem of environmental catalysis. Fuel combustion in diesel engines, power and heat plants, nitric acid factories and waste incinerators are the main sources of such off-gases [1] and [2].

The SCR of NO_x with ammonia is widely used for cleaning flue gases emitted by the power stations and chemical industrial plants. NH_3 is an expensive and corrosive reducer and is itself a pollutant. For off-gases of stationary sources of emission, NO_x reduction by hydrocarbons (HC) or direct NO decomposition both represent alternative methods of NO_x removal. The substitution of ammonia by methane seems to be economically attractive as it is non-corrosive and the most available hydrocarbon and thus the cheapest one. Methane is also quite neutral for the living organisms though it is a strong greenhouse gas [3], [4], [5] and [6]. Methane can be an internal reducer of NO_x in effluent gases of boilers using natural gas as a fuel. The temperature of NO

reduction decreases if NO is earlier oxidized to NO_2 [5], [7], [8], [9], [10], [11], [12] and [13]. It was shown that HCs are first oxidized by NO_2 to oxygenates.

Catalysts containing two noble metals, noble and non-noble transition metals or non-noble transition metal supported on zeolites [5], [7], [8], [9] and [14] or sulfated zirconia [10], [11] and [12] were investigated as promising catalysts for NO reduction by methane.

Mixed noble-metal-based catalysts (Ru, Rh, Pd, Ag, Ir, Pt and Au) supported on sulfated zirconia (SZ) were investigated in SCR of NO_x by methane in the presence of excess oxygen. It was shown that the most active catalyst contains 0.38 wt.% Pd and 0.12 wt.% Pt [10], [11] and [12].

Li et al. [11] examined catalysts containing transition metals (Co, Mn, In, Ni) supported on sulfated ZrO_2 (SZ). They found that the most active was the 4 wt.% Co/(SZ) catalyst, which yielded a conversion above 60% and showed good stability in a 60 h test.

Pd–Co/SZ catalysts with various Pd and Co loadings were studied by Cordoba et al. [12]. The 2.1 wt.% Co–0.06 wt.% Pd/SZ catalyst showed the highest activity.

Co–Pd catalysts supported on zeolites were investigated by Lee et al. [5] and Djéga-Mariadassou [14]. Co–Pd/Mordenite showed high activity in the temperature range 443–613 K [14]. The Co/Ferrierite catalyst with the addition of Pd showed higher activity in the temperature range 573–873 K than Co/Ferrierite catalysts with the addition of Pt, Ir, La or In. The deactivation of the Co–Pd/Ferrierite catalyst was rather slow even in the presence of water vapor [5]. Resini et al. [7] examined the influence of the support on the cobalt catalyst activity. The Co/MFI catalyst revealed higher activity than a Co/Ferrierite one. Burch and Scire [15] have observed NO decomposition on reduced metallic or metal ions sites of Cu-, Co-, Rh- and Pt-ZSM5 catalysts in the methane presence. This decomposition was accompanied by sites poisoned by oxygen, which was next removed by reduction with hydrocarbons.

Indium catalysts exhibit the highest activity in NO reduction by CH_4 among all the investigated systems containing transition non-noble metals. The H-ZSM5 supported catalysts were studied by Wang et al. [8] and Ren et al. [9]. Modifications in In/H-ZSM5 catalysts with Fe_2O_3 [8] or Al_2O_3 [9] resulted in increased activity. According to the authors [8] and [9] the presence of Al_2O_3 promotes the formation of NO_2 and increases methane activation.

A WO_3–ZrO_2 supported palladium catalyst was the subject of studies conducted by Okumura et al. [4]. The catalyst showed relatively high and stable activity in the presence of 10% water vapor.

Bimetallic 1.40 wt.% Pt–0.06 wt.% Rh catalyst used by Lyman and co-workers [16] exhibited high activity in NO reduction by H_2 or CO. The authors ascribed catalyst activity to homogenous Pt–Rh alloy formation.

Mechanisms of NO decomposition on Rh and Pt are widely discussed in Garin's review [17]. Platinum, rhodium and palladium supported on oxides are known to be the most active catalysts in NO decomposition [17], [18], [19], [20], [21], [22], [23], [24], [25], [26], [27], [28], [29], [30] and [31].

Gorte et al. [18] and Sugisawa et al. [19] examined the NO adsorption and decomposition over Pt monocrystals. Gorte et al. [18] have found that Pt(100) is exceptionally active in NO decomposition even at room temperature. Sugisawa et al. [19] have claimed that about half of the NO adsorbed on Pt(112) decomposed to N_2 at 383 K. Pt(111) and Pt(110) were found to be non-active in NO dissociation [18] and [19]. Pt(112) is nominally constructed from (110) step sites and (111) terrace sites. Sugisawa has found that NO adsorbs molecularly on Pt(112) at 95 K then about half of the NO molecules adsorbed on step sites decomposes at 483 K.

Wang et al. [20] have studied the influence of particle size and the support on NO decomposition over Pt supported on SiO_2, Al_2O_3, TiO_2 and MgO. They found NO decomposition over Pt/SiO_2 catalyst at 873 K insensitive to particle size and observed an absence of support effect on NO decomposition activities for Pt/SiO_2, Pt/Al_2O_3 and Pt/TiO_2. On the contrary, the NO decomposition activity of Pt supported on strongly basic MgO was found to be significantly lower.

Ishii et al. [21] investigated desorption states of nitric oxide, dioxygen and dinitrogen on Rh(100) surface. Two states of atomic oxygen were observed after NO adsorption and dissociation: an adatom state and oxidic state. The other state is NO molecule adsorbed on this surface. They suggested that N_2 desorbing at around 300 K is formed by the reaction of the nitrogen adatoms with the adsorbed NO molecules and nitrogen desorbed at around 560 K is formed by the reaction of two adatoms species of nitrogen.

An oxygen adsorption study on Rh(100) was carried out by Ueda et al. [22]. They reported three oxygen adsorption states: one inactive and two active.

Ho and White [23] reported that a low temperature desorption peak and three high desorption peaks were observed in the TPD spectra of nitrogen following the NO adsorption on Rh(100) at 100 K. They claimed that the recombination of adatoms was responsible for the highest temperature desorption. Root et al. [24] reported that at higher NO coverage on Rh(111) a new desorption state appears at 470 K. They stated that one possible mechanism for the desorption is the reaction of adsorbed NO with an adatom nitrogen. They also claimed that behaviour of NO adsorption and decomposition on Rh(111) is qualitatively similar to that on Rh(100). Major difference between Rh(111) and Rh(100) is the stronger bonding of nitrogen from NO decomposition on Rh(100), with the N_2 recombination peak occurring above 700 K on Rh(100) and at 560 K on Rh(111) [25].

Kondarides et al. [26] have observed 100% NO reduction by CO in the presence of O_2 at 573 K over Rh/TiO_2. They have shown that the process occurs via NO decomposition and removal of the forming oxygen adatoms by CO.

Almusaiteer et al. [27] have studied NO decomposition process at 673 K over Rh and Pd catalysts supported on alumina and carbon. They have observed poisoning of the Rh/Al_2O_3 and Pd/Al_2O_3 with the oxygen originating from NO decomposition. However, catalysts supported on carbon were much more stable because of the migration of oxygen adatoms to the carbon support. In the case of the Rh/C, CO_2 was formed as a result of carbon interaction with oxygen adatoms. However, in the case of Pd/C, carbon served only as an oxygen adsorbent.

Papp and Sabde [28] have investigated the influence of the preparation method on the dissociation activity of the Rh/SiO_2 at 373–673 K. They used a pulse reactor after decomposition of NO, with hydrogen pulse being used as an oxygen adatom scavenger. They found that at higher temperatures O_2 competes with NO for the same active sites. They also observed that N_2O was formed only for the high rhodium dispersion.

Nakatsuji and Komppa [29] have studied NO_x reduction on Rh supported catalysts in lean and rich operations and confirmed that Rh promotes the reduction of NO to N_2 even in the presence of SO_2.

Rahkamaa and Salmi [30] have studied the decomposition of NO on Rh/Al_2O_3 and concluded that N_2O is the necessary intermediate for NO decomposition to nitrogen.

Hanaoka et al. [31] have found that the synthesis procedure of Rh supported catalysts, which determines catalyst structure and chemical surface composition, plays a crucial role in the performance of these catalysts.

Comparison of NO dissociation on the (100) and (111) surfaces of Pt and Rh revealed that Rh is more active than Pt [18]. Recently it was found the formation of the surface Al_9Rh_2 nanocrystallites during the reduction of high-surface area alumina supported rhodium catalyst [32].

The aim of this paper was to investigate the correlation between the activity of the high surface alumina supported Rh, Pt, and Pt–Rh catalysts in NO conversion to N_2 and the surface structure.

The surface structure of the catalysts was investigated by HRTEM and the chemical composition of their surface nanolayer was determined by XPS. The catalysts' activity was investigated using transient (TPSR) as well as steady-state methods. It was expected that the Pt–Rh alloying effect reported by Lyman and co-workers [16] for CO and H_2 SCR would be observed.

2. Experimental

2.1. Catalysts preparation

High surface area alumina was obtained with the sol–gel method; 20.7 cm^3 aluminum tri-sec butoxide (>97%, Merck-Schuchardt) was slowly purred to 200 cm^3 of deionized water at 353 K. About 0.3 cm^3 of concentrated nitric acid was then added for peptization. An obtained sol solution was kept at 353 K under stirring for 2 h. The solutions of H_2PtCl_6, and/or $RhCl_3{\cdot}3H_2O$ in water were next added to the alumina sol solution. The catalyst precursor was calcined in air at 773 K for 3 h. At the end of the synthesis procedure the sample was reduced in a hydrogen stream at 573 K for 2 h and at 773 K for 1 h.

2.2. Catalysts' characterization

To characterize the catalysts, specific BET surface area, chemical composition of the surface nanolayers and phase composition were determined.

The specific BET surface area was measured by N_2 adsorption at 77.35 K using ASAP 2010 MICROMETRICS instrument.

X-ray photoelectron spectroscopy (XPS) was used to determine the chemical composition of the surface nanolayers for the freshly prepared catalysts. The measurements were conducted using an ESCA system 150 Vacuum Science Workshop with an aluminum anode as an X-ray source resulting in a surface sensitivity of approximately 2 nm. Rh 3d, Al 2p and Pt 4f binding energies were determined using the Al^{3+} 2p binding energy with 74.5 eV as a reference [33]. The phase composition of catalysts was determined by powder X-Ray Diffraction (XRD) on Siemens D 500 diffractometer with CuK_α radiation.

High-resolution electron images of the freshly prepared catalysts were acquired to determine phase composition in nanoareas of the catalysts. The HRTEM studies were conducted in a Philips CM 200 FEG instrument operated at 200 kV and equipped with a Gatan Image Filter (GIF) and CCD camera. The specimens for HRTEM were prepared by the dispersion a small amount of the samples in methanol and depositing them on holey carbon films supported on copper grids.

2.3. TPD of NO and catalytic activity measurements

Temperature-programmed desorption (TPD) experiments were performed in a quartz reactor. The adsorption was conducted in a gas mixture containing 150 ppm NO, 7% O_2 and argon as a balance at room temperature for 1 h. After the adsorption the reactor was purged with argon at room temperature until NO reached zero signal. TPD measurements were carried out up to 772 K, with the heating rate 3 K/min. in the mixture composed of 7% O_2 in argon. The GHSV was equal to 20,000 h^{-1}.

NO and NO_2 concentrations were determined simultaneously by Eco Physics CLD 700 AL NO_x chemiluminescence analyzer and an Ultramat 6 Siemens IR analyzer was used to monitor N_2O.

The catalytic activity measurements were performed under transient as well as steady-state conditions in a quartz reactor. The feed gas mixture consisted of 150 ppm NO, 1500 ppm CH_4, 7% O_2 and Ar as a balance was used in both cases. The gas hour space velocity (GHSV) was equal to 20,000 h^{-1}. The heating rate was maintained at 3 K/min.

Before the TPSR, the catalyst was pretreated in flowing argon at 773 K for 1 h, with the heating rate 10 K/min, whereas before the steady-state experiment it was annealed in the reaction mixture and consecutive measurements were performed stepwise starting from 773 to 473 K.

A FID detector was used to follow the total concentration of hydrocarbons (HC) and the N_2 formation over Rh/Al_2O_3 catalyst was checked by micro-GC.

3. Results and discussion

The contents of the metal atoms and ions in the surface nanolayers determined from XPS spectra as well as the specific BET surface area of the catalysts are summarized in Table 1. The total amount of the metal atoms and cations were taken as 100%. The fact that the rhodium content in the surface nanolayer of the 0.03 at.% Rh/Al_2O_3 (0.06 wt.% Rh/Al_2O_3) catalyst is higher than the platinum content in the surface nanolayer of 0.51 at.% Pt/Al_2O_3 (1.56 wt.% Pt/Al_2O_3) can be explained by the different ways that Rh and Pt are deposited on the surface. The Rh cations are probably deposited by exchange with protons of the Brönsted acidic OH groups, while $[PtCl_6]^{2-}$ anions are partially exchanged with the basic OH groups and partially impregnated. The higher platinum exposition on the 0.34 at.% Pt–0.03 at.% Rh/Al_2O_3 (1.03 wt.% Pt–0.05 wt.% Rh/Al_2O_3) catalyst surface than on the 0.51 at.% Pt/Al_2O_3 one suggests that some $[PtCl_6]^{2-}$ anions undergo adsorption on earlier deposited Rh^{3+} cations. This suggests that the clusters composed of both precious metal atoms are probably formed during the next stage of the Pt–Rh catalyst synthesis. Metallic and ionic species are present in the surface nanolayers of all the catalysts. Metallic species prevailed in the surface nanolayers of 0.03 at.% Rh/Al_2O_3 catalyst, while ionic ones in 0.51 at.% Pt/Al_2O_3 and 0.34 at.% Pt–0.03 at.% Rh/Al_2O_3 catalysts.

Table 1. Pt and/or Rh contents in the bulk and in the surface nanolayers of the Pt/Al_2O_3, Rh/Al_2O_3 and $Pt–Rh/Al_2O_3$ catalysts and the catalyst specific BET surface areas

Catalyst	**Pt and/or Rh (bulk) (at.%)**	**Pt and/or Rh (surface) (at.%)**	**Pt^0 and/or Rh^0**	**Pt^{2+}**	**Pt^{4+}**	**Rh^{3+}**	**Rh^{4+}**	**BET surface area (m^2/g)**
Pt	0.51	0.4	0.1	0.2	0.1			283
Rh	0.03	0.7	0.4			0.2	0.1	330
Pt–Rh	0.34Pt + 0.03Rh	0.5Pt + 0.5Rh	0.1Pt + 0.2Rh	0.4		0.2	0.1	302
Al_2O_3								287

The specific BET surface areas of all the catalysts are quite close. The largest specific BET surface area of Rh catalyst suggests that rhodium hinders alumina crystallization.
Fig. 1 shows XRD pattern of the Rh/Al_2O_3 catalyst which match well to one of δ-alumina [34].

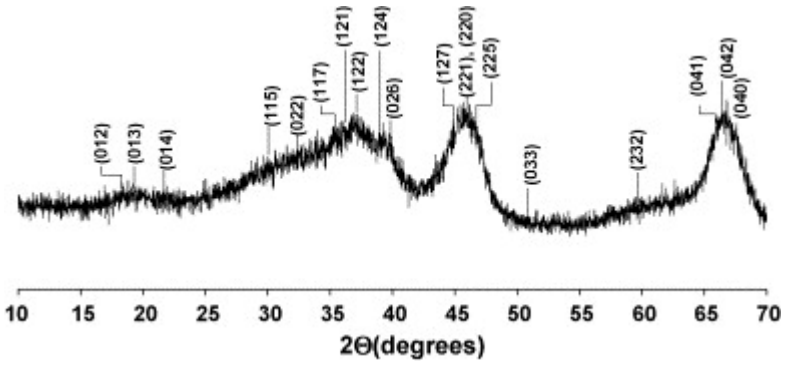

Fig. 1. XRD pattern of the Rh/Al_2O_3 catalyst (δ-alumina hkl).

In Fig. 2 HRTEM representative image of the Rh/Al_2O_3 catalyst is presented. The crystalline areas of Al_9Rh_2 [35] are well seen. In the Pt/Al_2O_3 and $Pt–Rh/Al_2O_3$ catalyst the crystalline Al_2Pt alloy was found [36]. It is obvious that the Al_2Pt phase revealed in the bimetallic Pt–Rh catalyst also contains rhodium. The presence of the relatively small crystallites in the Rh/Al_2O_3 catalyst is associated with incorporation of the Rh^{4+} ions, with the ionic radius close to that of Al^{3+} (r_{Rh4+} = 0.60 Å and r_{Al3+} = 0.54 Å — octahedral coordination in δ-alumina phase [37]), as discussed elsewhere [32]. Rh ions in alumina lattice retard growth of the alumina crystallites and facilitate alumina reduction, which leads to Al_9Rh_2 alloy, due to the formation of cationic vacancies [32]. On the other hand, platinum does not incorporate so easily into alumina due to its larger ionic radius (r_{Pt4+} = 0.63 Å [37]) and nor does it distinctly change alumina crystallinity. These observations are consistent with differences in the specific BET surface area of particular catalysts. We did not notice the presence neither Rh particles nor Pt–Rh alloy crystallites demonstrated by Lakis et al. for catalysts of similar compositions [38].

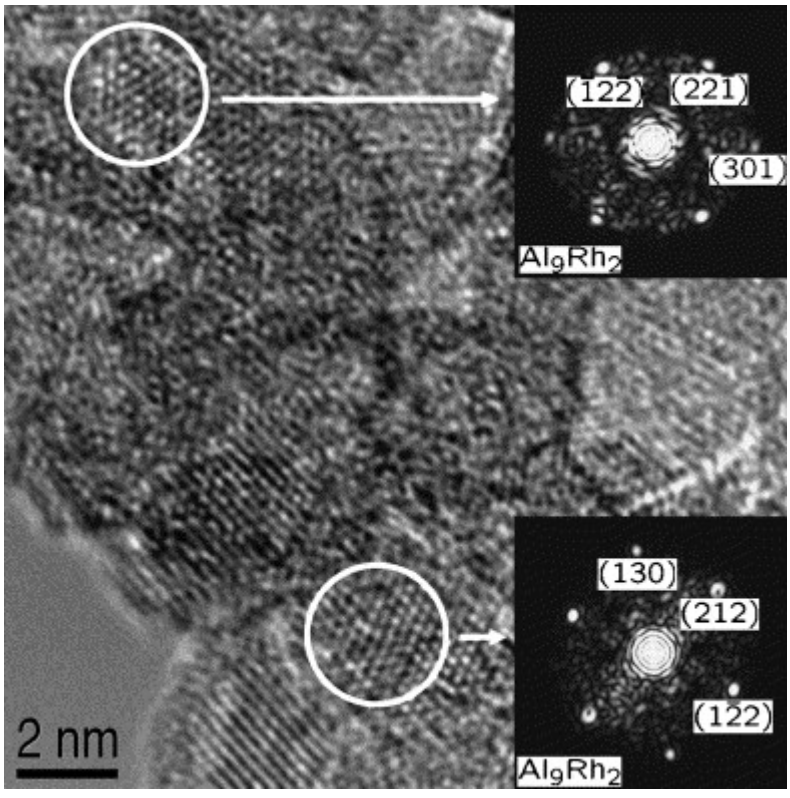

Fig. 2. HRTEM image of the Rh/Al_2O_3 catalyst with the marked areas of the crystalline Al_9Rh_2 alloy.

Fig. 3 shows TPD profiles of NO, NO_2 as well as NO + NO_2 from the Rh/Al_2O_3 (A), Pt/Al_2O_3 (B) and $Pt–Rh/Al_2O_3$ (C) catalysts and Al_2O_3 support (D). In all cases, two groups of NO_x, NO and NO_2 desorption peaks are present, a fact which may be attributed to the presence of two different phases adsorbing nitrogen oxides with different strengths. Both groups of peaks of all the catalysts are distinctly shifted towards lower temperatures in comparison with those of the alumina support. This indicates that precious metals are incorporated in both adsorbing phases, changing their adsorptive properties. Comparing the peaks' positions allows us to conclude that the temperature of NO desorption from the metallic phase is lower than that of NO_2. On the contrary NO_2 desorbs at lower temperatures than NO does from the oxide phase (Fig. 3A–C). It may be concluded that on alloys, NO is adsorbed on precious metal (PM) atoms and NO_2 on oxygen species formed on Al atoms. However, in the oxidic phase NO may strongly adsorb in the oxygen vacancies and NO_2 may be formed due to NO adsorption on oxygen species on bare aluminum ions. The great shift of the first peaks of the Pt-containing catalysts towards lower temperatures with respect to alumina confirms that platinum forms surface alloy with relatively high platinum content. The much smaller shift of the first group of peaks in the case of the Rh/Al_2O_3 catalyst coincidence well with lower rhodium content in Rh–Al alloy.

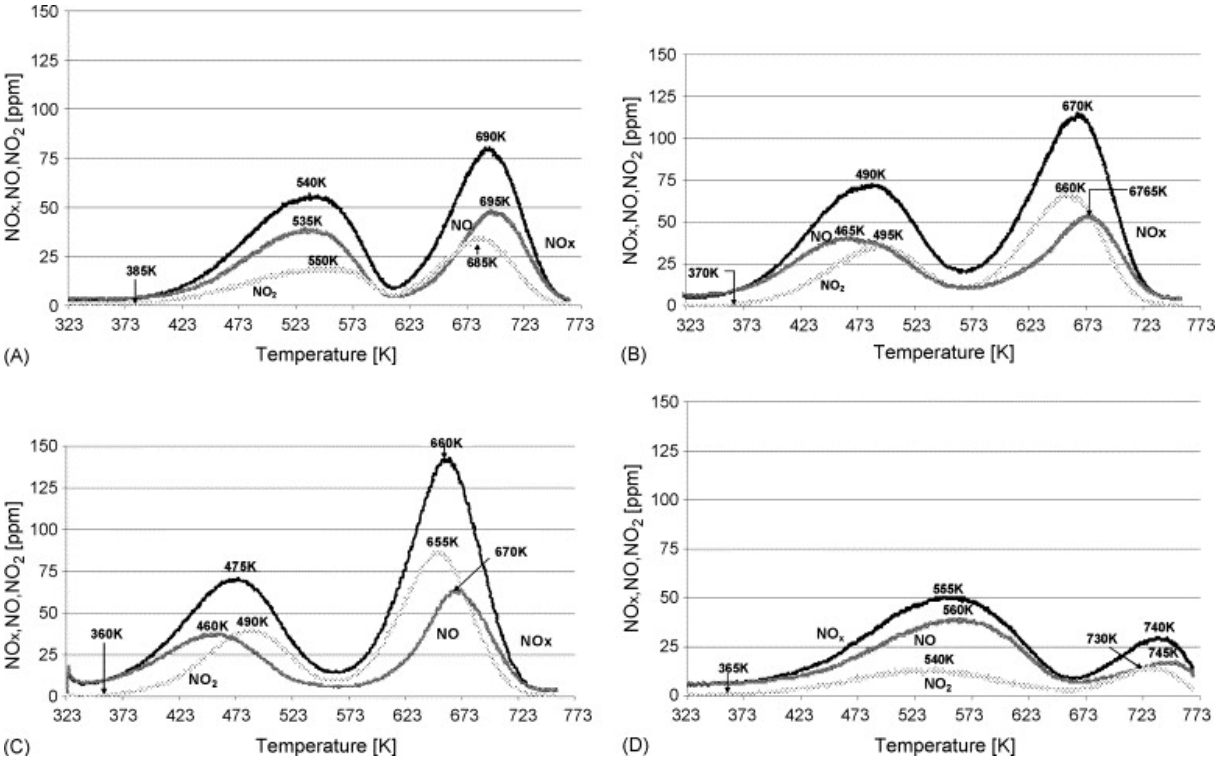

Fig. 3. Temperature-programmed NO_x desorption profiles in O_2 after exposure of the catalysts to gas mixture containing 150 ppm NO, 7% O_2 and argon as a balance at room temperature for 1 h; Rh/Al_2O_3 (A), Pt/Al_2O_3 (B), $Pt–Rh/Al_2O_3$ (C) and Al_2O_3 (D). GHSV = 20,000 h^{-1}, heating rate maintained at 3 K/min.

In Fig. 4, TPSR profiles for Rh/Al_2O_3 (A), Pt/Al_2O_3 (B), $Pt–Rh/Al_2O_3$ (C) and Al_2O_3 support (D) are shown. It should be emphasized that N_2O was not detected at any temperature and therefore the N_2O profile was omitted. As in TPD profiles, two groups of peaks of nitrogen oxides are here easily recognizable. However, whereas the peaks connected with oxide phase occur approximately at the same temperature ranges on TPSR and on TPD profiles, the TPSR peaks connected with metallic phase are distinctly shifted towards higher temperature with respect to TPD ones. Beyond these two groups of peaks, the asymmetric low-temperature NO peaks centered in the 353–418 K range of temperature appeared. The shift of the alloy-derived TPSR peaks towards higher temperatures with respect to TPD ones may only be explained if the

occurrence of the direct decomposition of NO to N_2 and O_2 is taken into account. Thus, one may be led to believe that the low temperature NO peaks, not having counterparts in TPD profiles, are artificially formed from the left shoulders originating from a decrease in the rate of NO adsorption and the right ones illustrating an increasing rate of NO decomposition.

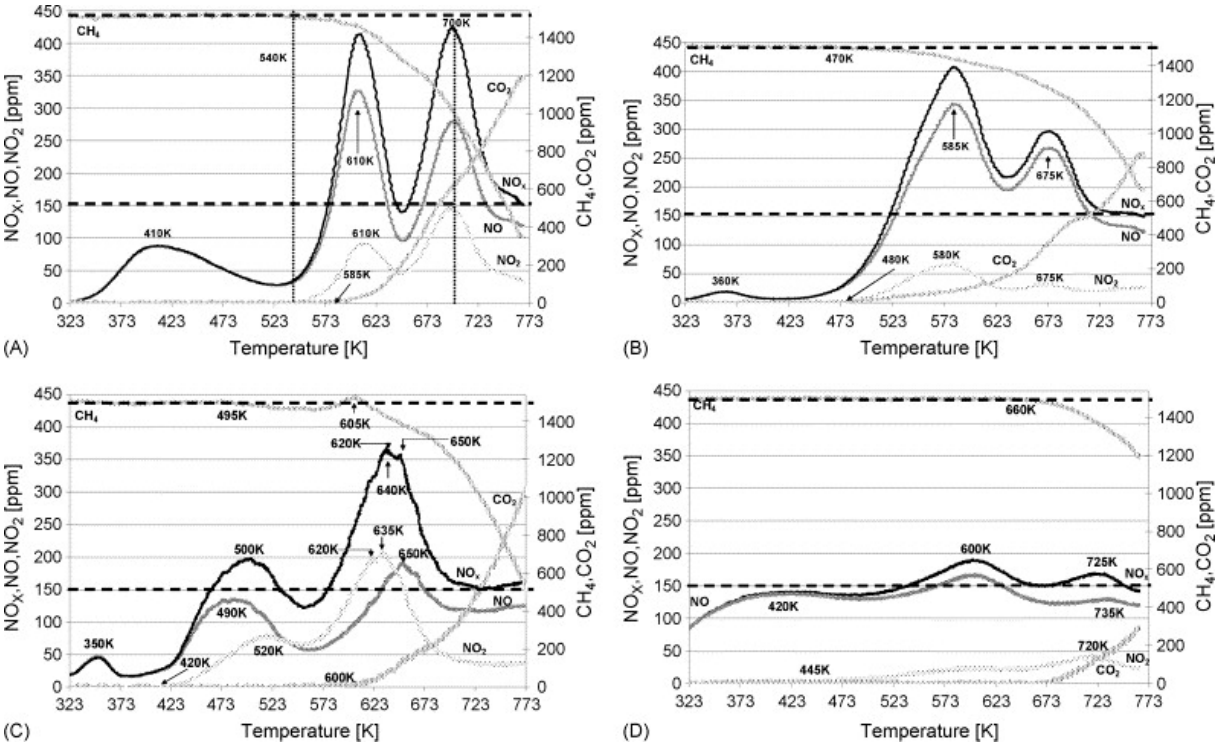

Fig. 4. Temperature-programmed surface reaction profiles after exposure of the catalysts to gas mixture containing 150 ppm NO, 7% O_2, 1500 ppm CH_4 and argon as a balance in the temperature range 323–773 K. Rh/Al_2O_3 (A); Pt/Al_2O_3 (B); $Pt–Rh/Al_2O_3$ (C); Al_2O_3 (D). GHSV = 20,000 h^{-1}, heating rate maintained at 3 K/min.

The initial temperature of the methane activation, and its subsequent oxidation to CO_2, is the lowest (470 K) for the Pt/Al_2O_3 catalyst and the highest (660 K) for the alumina support. Over the $Pt–Rh/Al_2O_3$ catalyst, methane consumption begins at 495 K but is not initially followed by CO_2 formation. Methane activation followed by CO_2 formation starts only at 605 K. One may conclude that CH_4 molecules undergo oxidation by oxygen species adsorbed on Al atoms. The presence of the precious metal clusters on the surface of Pt–Rh–Al alloy in the bimetallic catalyst makes physical methane adsorption possible (Fig. 4C). The adsorbed CH_4 molecules start to be oxidized at higher temperatures after gaining sufficient energy to migrate to oxygen active species on aluminum atoms.

In the case of the Pt/Al_2O_3 catalysts, the amount of NO_2 desorbed during TPSR is much smaller than during TPD. This suggests that NO_2 is used for CH_4 oxidation. Following the shape of the CO_2 curve, one can conclude that CH_4 oxidation has two temperature ramps; total methane oxidation to CO_2 at lower temperatures, demonstrated by the CO_2 curve with a big slope to temperature axis as well as partial CH_4 oxidation, illustrated by the segment of the CO_2 curve, which is almost parallel to the temperature axis. It may also be concluded that molecules of $NO_{2(ads.)}$ of relatively high concentration cause total methane oxidation to CO_2, while those of relatively small concentration result in partial CH_4 oxidation. At the same time a distinct decrease in the ratio of the NO amounts desorbed from oxidic and metallic phases with respect to that in TPD suggests that in the course of TPSR NO is partially reduced by the products of partial methane oxidation. A similar but less evident effect is observed on the CO_2 curve for the Rh/Al_2O_3 and $Pt–Rh/Al_2O_3$ catalysts. The HC-deNO_x mechanism involving CH_4 oxidation by

NO_2 to oxygenates and the subsequent NO reduction by those oxygenates was earlier proposed by Djéga-Mariadassou [14].

NO conversion (C_{NO}), selectivity to N_2 (S_{N2}) and N_2 yield (N_2), calculated from the results of the steady-state experiments over the Rh/Al_2O_3 (A), Pt/Al_2O_3 (B) and $Pt–Rh/Al_2O_3$ (C) catalysts, are presented in Fig. 5. It should be noted that NO conversion at 473 K over the Rh/Al_2O_3 catalyst was not stable and therefore it is not presented in Fig. 5a and c.

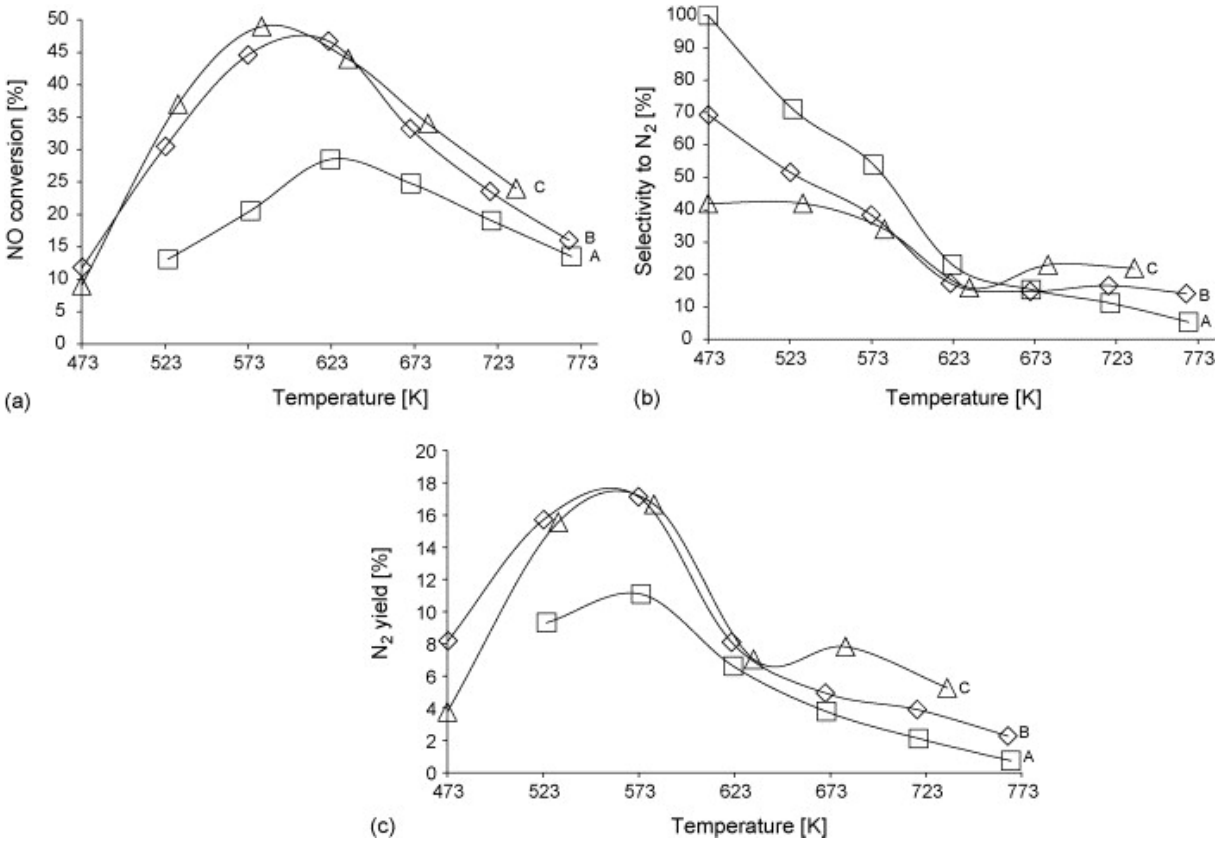

Fig. 5. NO conversion (C_{NO} (a)), selectivity to N_2 (S_{N2} (b)) and N_2 yield (N_2 (c)) calculated from the results of the steady-state experiment over; (□) Rh/Al_2O_3 (A); (◊) Pt/Al_2O_3 (B); (Δ) $Pt–Rh/Al_2O_3$ (C). The feed gas mixture consisted of 150 ppm NO, 1500 ppm CH_4, 7% O_2 and Ar as a balance was used; the experiments were performed in the direction from 773 to 473 K after TPSR ones. GHSV = 20,000 h^{-1}, heating rate maintained at 3 K/min.

As mentioned in Section 2, steady-state experiments were performed in the direction from 773 to 473 K after the TPSR ones. Activity of the catalysts towards NO decomposition observed at temperatures lower than 623 K shows that the sites active in this process do not undergo poisoning by the reagents. Therefore, it is reasonable to assume that the PM atoms of the alloy phases are the active sites in the low temperature NO decomposition. A comparison of C_{NO}, S_{N2} and Y_{N2} curves reveals that the NO decomposition over alloy phases stops earlier than the NO oxidation. This may occur because the NO adsorption on PM atoms stops at a lower temperature than the oxygen adsorption on aluminum atoms of alloys. The NO oxidation that occurs on δ-alumina phase not followed by $deNO_x$ can also be a factor in the difference in shape between C_{NO} and Y_{N2}. As mentioned above, the slight CH_4 $deNO_x$, observed above 623 K occurs on δ-alumina phase due to NO reduction with oxygenates and is formed by the partial methane oxidation with NO_2 adsorbed.

It should be emphasized here that N_2 formation over the Rh/Al_2O_3 catalyst was confirmed in the whole range of temperature by micro-GC, but is not shown here.

Unlike Rahkamaa and Salmi [30], who claimed that N_2O is the intermediate for NO decomposition to N_2 over an Rh/Al_2O_3 catalyst, we did not observe at all the formation of N_2O. Thus, we agree with Almusaiteer et al. [27] who found that NO decomposition over an alumina supported rhodium catalyst occurs according to the equation: $Rh + 2NO \rightarrow 2Rh–O +,N_2$. Wang et al. [20] claimed that low temperature NO decomposition in the absence of oxygen over an alumina supported platinum catalyst initially yields N_2 and N_2O and results in rapid catalyst deactivation due to oxygen poisoning. The absence of rapid catalyst deactivation by oxygen adsorption over our Rh/Al_2O_3 catalyst may be attributed to the migration of oxygen from rhodium to aluminum atoms. Suppression of Rh poisoning by oxygen due to oxygen migration to support was earlier observed by Almusaiteer et al. [27] for a Rh/C catalyst.

4. Conclusions

0.03 at.% Rh/Al_2O_3, 0.51 at.% Pt/Al_2O_3 and 0.34 at.% Pt–0.03 at.% Rh/Al_2O_3 catalysts were obtained, respectively, by cationic exchange of Rh^{3+} with protons of the acidic alumina OH groups, anionic exchange of $[PtCl_6]^{2-}$ with basic OH groups of alumina and both cationic and anionic exchange. All the catalysts contained δ-alumina with incorporated precious metal atoms and Rh–Al, Pt–Al and Pt–Rh–Al phases—isostructural with Al_9Rh_2 and Al_2Pt alloys. They were investigated as possible catalysts for NO conversion to N_2 in the presence of oxygen and methane. Each of them showed reasonable low temperature activity in direct NO decomposition to N_2 and O_2 over alloy phases at the temperature ranges 410–623, 360–623 and 350–623 K, respectively. At temperatures above 623 K some CH_4 $deNO_x$ on δ-alumina with some precious metal cations was also observed. It was suggested that NO first adsorbs on precious metal atoms and next undergoes decomposition due to electron transfer to nitric oxide antibonding π orbitals. One hundred percent selectivity to N_2 was observed over Rh/Al_2O_3 when oxygen active species on aluminum atoms did not have a role in NO conversion. It was demonstrated that CH_4 $deNO_x$ occurs according to Djéga's mechanism based on CH_4 oxidation by NO_2 to oxygenates, which were subsequently employed to reduce NO.

References

[1] X. Gao, Q. Yu and L. Chen, *J. Natural Gas Chem.* **12** (2003), p. 264.

[2] A. Fritz and V. Pitchon, *Appl. Catal. B* **13** (1997), p. 1.

[3] R.M. Heck, R.J. Farrauto and S.T. Gulati, Catalytic Air Pollution Control Commercial Technology, Wiley–Interscience (2002) pp. 72–311.

[4] K. Okumura, T. Kusakabe and M. Niwa, *Appl. Catal. B* **41** (2003), p. 137.

[5] T.J. Lee, I.-S. Nam, S.-W. Ham, Y.-S. Baek and K.-H. Shin, *Appl. Catal. B* **41** (2003), p. 115.

[6] V.I. Pârvulescu, P. Grange and B. Delmon, *Catal. Today* **46** (1998), p. 233.

[7] C. Resini, T. Montanari, L. Nappi, G. Bagnasco, M. Turco, G. Busca, F. Bregani, M. Notaro and G. Rocchini, *J. Catal.* **214** (2003), p. 179.

[8] X. Wang, T. Zhang, X. Sun, W. Guan, D. Liang and L. Lin, *Appl. Catal. B* **24** (2000), p. 169.

[9] L. Ren, T. Zhang, J. Tang, J. Zhao, N. Li and L. Lin, *Appl. Catal. B* **41** (2003), p. 129.

[10] H. Ohtsuka, *Appl. Catal. B* **33** (2001), p. 325.

[11] N. Li, A. Wang, J. Tang, X. Wang, D. Liang and T. Zhang, *Appl. Catal. B* **43** (2003), p. 195.

[12] L.F. Cordoba, W.M.H. Sachtler and C.M. de Correa, *Appl. Catal. B* **56** (2005), p. 269.

[13] H. Ohtsuka and T. Tabata, *Appl. Catal. B* **29** (2001), p. 177

[14] G. Djéga-Mariadassou, *Catal. Today* **90** (2004), p. 27.

[15] R. Burch and S. Scire, *Appl. Catal. B* **3** (1994), p. 295.

[16] R.E. Lakis, Y. Cai, H.G. Stenger and Ch.E. Lyman, *J. Catal.* **154** (1995), p. 276.

[17] F. Garin, *Appl. Catal. A* **222** (2001), p. 183.

[18] R.J. Gorte, L.D. Schmidt and J.L. Gland, *Surf. Sci.* **109** (1981), p. 367.

[19] T. Sugisawa, J. Shiraishi, D. Machihara, K. Irokawa, H. Miki, C. Kodama, T. Kuriyama, T. Kubo and H. Nozoye, *Appl. Surf. Sci.* **169/170** (2001), p. 292.

[20] X. Wang, S.M. Sigmon, J.J. Spivey and H.H. Lamb, *Catal. Today* **96** (2004), p. 11

[21] M. Ishii, T. Hayashi and S. Matsumoto, *Appl. Catal. A* **225** (2002), p. 207.

[22] K. Ueda, A. Takano and K. Tanaka, *Jpn. J. Appl. Phys.* **34** (1995), p. 3662.

[23] P. Ho and J.M. White, *Surf. Sci.* **137** (1984), p. 117.

[24] T.W. Root, L.D. Schmidt and G.B. Fisher, *Surf. Sci.* **134** (1983), p. 30.

[25] G.B. Fisher and S.J. Schmieg, *J. Vac. Sci. Technol. A* **1** (1983), p. 1064.

[26] D.I. Kondarides, T. Chafik and X.E. Verykios, *J. Catal.* **191** (2000), p. 147.

[27] K. Almusaiteer, R. Krishnamurthy and S.S.C. Chuang, *Catal. Today* **55** (2000), p. 291.

[28] H. Papp and D.P. Sabde, *Appl. Catal. B* **60** (2005), p. 65.

[29] T. Nakatsuji and V. Komppa, *Catal. Today* **75** (2002), p. 407.

[30] K. Rahkamaa and T. Salmi, *Chem. Eng. Sci.* **54** (1999), p. 4343.

[31] T. Hanaoka, W.Y. Kim, M. Kishida, H. Nagata and K. Wakabayashi, *Chem. Lett.* (1997), p. 645.

[32] M. Zimowska, J.B. Wagner, J. Dziedzic, J. Camra, B. Borzęcka-Prokop and M. Najbar, *Chem. Phys. Lett.* **417** (2006), p. 137.

[33] C.D. Wagner, W.M. Riggs, L.E. Davis, J.F. Moulder, G.E. Muilenberg, Handbook of X-ray Photoelectron Spectroscopy, Physical Electronics Division, Perkin-Elmer Corporation, Eden Prairie, Minnesota, 1979, available from: www.lasurface.com

[34] Y. Repelin and E. Husson, *Mat. Res. Bull.* **25** (1990), p. 611.

[35] L.E. Edshammar, *Acta Chem. Scand.* **22** (1968), p. 2822.

[36] A. Pietraszek, P. Da Costa, G. Djéga-Mariadassou, J.B. Wagner, P. Kornelak, M. Najbar, in preparation.

[37] Handbook of Chemistry and Physics, 85 ed., CRC Press, Boca Raton, 2004.

[38] R.E. Lakis, Ch.E. Lyman and H.G. Stenger, *J. Catal.* **154** (1995), p. 261.